



UNIVERSITY OF LEEDS

This is a repository copy of *Optimal Design of Series-Parallel Differential Power Processing Converters for Photovoltaic Array Energy Systems*.

White Rose Research Online URL for this paper:  
<http://eprints.whiterose.ac.uk/167293/>

Version: Accepted Version

---

**Proceedings Paper:**

Etarhouni, M [orcid.org/0000-0003-1626-2585](https://orcid.org/0000-0003-1626-2585), Chong, B and Zhang, L (2020) Optimal Design of Series-Parallel Differential Power Processing Converters for Photovoltaic Array Energy Systems. In: EU-PVSEC Proceedings 2020. 37th European Photovoltaic Solar Energy Conference and Exhibition, 07-11 Sep 2020, Lisbon. , pp. 1181-1187. ISBN 3-936338-73-6

<https://doi.org/10.4229/EUPVSEC20202020-4AV.3.7>

---

Protected by copyright. This is an author accepted version of a paper published in the EU PVSEC proceedings, uploaded in accordance with the publisher's self-archiving policy.

**Reuse**

Items deposited in White Rose Research Online are protected by copyright, with all rights reserved unless indicated otherwise. They may be downloaded and/or printed for private study, or other acts as permitted by national copyright laws. The publisher or other rights holders may allow further reproduction and re-use of the full text version. This is indicated by the licence information on the White Rose Research Online record for the item.

**Takedown**

If you consider content in White Rose Research Online to be in breach of UK law, please notify us by emailing [eprints@whiterose.ac.uk](mailto:eprints@whiterose.ac.uk) including the URL of the record and the reason for the withdrawal request.



[eprints@whiterose.ac.uk](mailto:eprints@whiterose.ac.uk)  
<https://eprints.whiterose.ac.uk/>

# OPTIMAL DESIGN OF SERIES-PARALLEL DIFFERENTIAL POWER PROCESSING CONVERTERS FOR PHOTOVOLTAIC ARRAY ENERGY SYSTEMS

Mohamed Etarhouni, Benjamin Chong, Li Zhang  
 University of Leeds, School of Electronic and Electrical Engineering,  
 Woodhouse lane, LS2 9JT, Leeds, UK  
[fy09mse@leeds.ac.uk](mailto:fy09mse@leeds.ac.uk), [b.chong@leeds.ac.uk](mailto:b.chong@leeds.ac.uk), [l.zhang@leeds.ac.uk](mailto:l.zhang@leeds.ac.uk)

**ABSTRACT:** A scheme is proposed for maximum power point tracking in series-parallel photovoltaic arrays using differential power processing, based on bidirectional Cuk converters and inverted buck converters for adjusting module current and voltage respectively. Converter transfer functions are derived using linearization and state space time averaging. These are used to develop design criteria for well-behaved transient response, and reduction of the effect of non-minimum phase. A representative design with about 10 ms settling is presented. It is shown that this can form the basis of a successful perturb-and-observe control system.

**Keywords:** SP PV array, Differential Power Processing (DPP), Transient response, MPPT tracking, Perturb & Observe

## 1 INTRODUCTION

Differential Power Processing (DPP) converters have recently gained significant research attention due to their ability to mitigate the mismatch effect on PV systems by only processing a differential power and thus reducing the system losses [1]. DPP converter architectures, i.e. series or parallel, were proposed using various converter circuit topologies [2-4], but the key challenge here in choosing a suitable DPP converter circuit scheme is to balance either currents or voltages while maintaining high quality power control under almost all-weather conditions. Bidirectional buck-boost or fly-back, and SEPIC, including inverted-buck converters, are popular choices for either series or parallel DPP schemes; however, the work in [5] has overcome the limitations of these two schemes using a combined approach, so-called Series-Parallel DPP (SP-DPP) converters for PV array systems, as seen in Fig. 1. In this system, a Bidirectional Cuk Converter (BCC) is preferred over buck-boost type since the latter leads to non-continuous input and output currents, and so requires large capacitors connected across the terminals of the PV modules. A BCC can also maintain the current balancing between the serially connected modules while the voltage equalisation between the parallel strings is achieved here using a cascaded Front-End and Inverted-Buck Converter (IBC) circuit topology [5].

On the other hand, SP-DPP converter systems are becoming more complex, having higher system order arising in several passive components. Thus, MPPT for such a system can create disturbances if the PV voltages are continuously perturbed without a feedback controller to dampen the system dynamics. For some PV systems, MPPT can be achieved without or with feedback controller; the former is simpler to design and thus is suitable for certain practical systems, such as those applied in rural and remote areas. [6] developed a unified modelling scheme for a BCC which has yielded its derived transfer functions. However, this method only focused on a single string having two PV panels in series; the effect of the parallel DPP dynamics was not considered. Further analysis by [4] used a simple design approach based on a state-space averaging method to simulate the behavior of parallel DPP converters, which were implemented using IBCs, but this work has not yet been applied to investigate the transient variations at different operating points. [7] recently employed a design procedure for parallel DPP converters based on bidirectional buck-boost topology, but

the method was somewhat complex. Hence, there is still little existing work studied the dynamics effect of the series and parallel DPP converters together on the transient performance of a PV array system. Moreover, it is difficult to design combination of series and parallel scheme comprising BCC and IBC. A selected set of values for BCC and IBC components may compromise the array system's steady state behavior or vice versa. The objective of this paper is to develop a unified coherent model scheme for the selection of SP-DPPs converter components which is accurate enough in representing the non-linear features of the array converters circuit.

This paper presents a detailed analysis of BCC and IBC circuits. Then, state-space averaging and small-signal ac perturbations were used to derive the transfer functions of both converter schemes. For this model, a novel design scheme was developed to design BCC and IBC leading to an optimal performance in their transient and steady states. The designed scheme is verified through simulation results. Also, the designed converters model was utilised to achieve a maximum power point tracking of a PV array. It worth mentioning that PI controller is avoided in this case, as the design and implementation of this controller can further complicate MPPT of the PV array. Therefore, the system is biased only towards fully (P&O) method, but this relies on a system with good transient responses, which have been already obtained using the optimal set of the BCC and IBC components.

## 2 SERIES-PARALLEL DIFFERENTIAL POWER PROCESSING (SP-DPP) CONVERTERS CIRCUIT

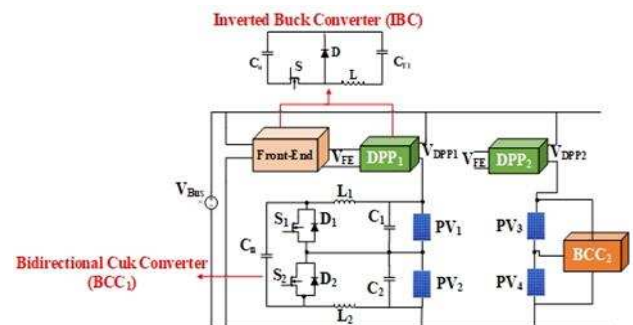


**Fig. 1:** SP-DPPs converters circuit scheme

Fig. 1 presents a practical PV array system, which has strings of serially connected modules along with additional chains interconnected in parallel. MPPT throughout this array requires adjustments of both module currents and string voltages, which was realised here by DPP processing using Bidirectional Cuk Converters (BCCs) for current balancing and Inverted Buck Converters (IBCs) for voltage balancing as seen in Fig. 1.

### 2.1 BCC circuit & operating principles

As shown in Fig.1, there are two pairs of switching devices for this converter, switch  $S_1$  – diode  $D_2$  and switch  $S_2$  – diode  $D_1$ . Only a single switch pair can be activated throughout a fixed operating condition. Two inductors  $L_1$  and  $L_2$  are at the sides of  $V_{PV1}$  and  $V_{PV2}$  respectively. Approximating the converter circuit as ideal, the internal resistance of the BCC components is negligible; device pairs whether  $S_1$ - $D_2$  or  $S_2$ - $D_1$  are turned on/off instantaneously, and losses of their on/off states are insignificant. The energy capacitor  $C_n$  is the crucial element in this circuit and is used to transfer the energy from  $V_{PV1}$  to  $V_{PV2}$  or vice versa depending on which side acts as the input terminal. Capacitors  $C_1$ ,  $C_n$  and  $C_2$  are assumed to be sufficiently large; hence, fluctuations of  $V_{PV1}$ ,  $V_{CN}$  and  $V_{PV2}$  around their average levels will be small. Also, with high enough switching frequency, the inductor currents  $i_{L1}$  and  $i_{L2}$  are considered as varying linearly with the time throughout a switching period. The following analysis is accomplished by using smoothed currents and voltages considered as instantaneous averaged values over one switching period. Thus, in the steady state, voltages across the two inductors,  $V_{L1}$  and  $V_{L2}$  are zero such that,

$$V_{CN} = V_{PV1} + V_{PV2} \quad (1)$$

Continuous Conduction Mode (CCM) is considered in the steady state. The switching pair  $S_1$ - $D_2$  is active, and the duty ratio is  $K_{11}$ , i.e.  $V_{PV1}$  is the input; hence, the energy is transferred from  $V_{PV1}$  to  $V_{PV2}$ . When  $S_1$  is turned on at time interval  $t_{on}$ ,  $D_2$  is reverse biased by  $V_{CN}$ ,  $L_1$  is charged by energy from  $V_{PV1}$ , causing  $i_{L1}$  to increase linearly.  $C_n$  discharges energy to  $V_{PV2}$  and  $L_2$  through  $S_1$ , resulting in the current  $i_{L2}$  rising linearly. When  $S_1$  is turned off,  $D_2$  becomes forward-biased,  $L_1$  supplies energy to  $C_n$  while energy is supplied to  $V_{PV2}$  by  $L_1$ . Therefore, both  $i_{L1}$  and  $i_{L2}$  increase linearly. In the steady-state operation, the net change in inductor current is zero; hence, the voltage-time balance equations for  $L_1$  and  $L_2$  respectively are given by:

$$\text{and} \quad \frac{V_{PV1}K_{11} + (V_{PV1} - V_{CN})(1 - K_{11})}{(V_{CN} - V_{PV2})K_{11} - V_{PV2}(1 - K_{11})} \quad (2)$$

The relationship between  $V_{PV1}$  and  $V_{PV2}$  is given by eliminating  $V_{CN}$  as:

$$\left| \frac{V_{PV1}}{V_{PV2}} \right| = \frac{K_{11}}{1 - K_{11}} \quad (3)$$

For lossless circuit elements, the current relationships can be written as:

$$\left| \frac{I_{L2}}{I_{L1}} \right| = \frac{1 - K_{11}}{K_{11}} \quad (4)$$

### 2.2 Operating principles of Inverter Buck Converter (IBC)

Fig.2 presents the circuit schematic of DPP converters,

which is composed of cascaded connection between front-end and DPP<sub>1</sub> converters. Hence, the latter is primarily implemented using Inverted Buck Converter (IBC) topology.

The four active components in the above IBC circuit are front-end switch  $S_F$  along with its associated diode  $D_F$ , and DPP<sub>1</sub> switch  $S$ , including its diode  $D$ , leading to four operating modes.

The input voltage to the front-end converter is  $V_{Bus}$ , and the output of this converter is the voltage across  $C_{TF}$  (i.e.  $V_{fe}$ ). Thus,  $V_{fe}$  is the common input to the other two DPP converters, DPP<sub>1</sub> and DPP<sub>2</sub>. The DPP<sub>1</sub> output voltage across the capacitor  $C_{T1}$  (i.e.  $V_{DPP1}$ ) is measured by taking the difference between the  $V_{Bus}$  and the total MPP voltage of the BCC<sub>1</sub> unit (i.e.  $V_{T1}$ ) within the first string. Output capacitors, including  $C_o$  and  $C_F$  function as an output filter. Therefore, the power is supplied from the input source on the right side of the IBC to the bus side through a two-stage power conversion using front-end and DPP<sub>1</sub> converters.

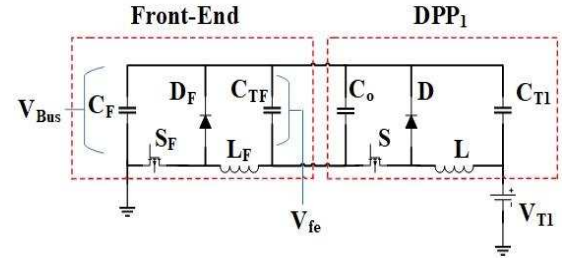


Fig. 2: Schematic of IBC circuit

Following the CCM analysis, when  $S_F$  and  $S$  are both turned on,  $D_F$  and  $D$  are reverse-biased, and the energy is directly supplied from  $V_{T1}$  to the bus voltage side  $V_{Bus}$  through  $L$  and  $L_F$  provided that the source current is grounded. When  $S_F$  is turned on, and  $S$  is off,  $D$  now becomes forward-biased while  $D_F$  is reverse-biased; thus,  $L$  supplies energy to  $C_F$ . For the next operating mode when  $S_F$  is turned off, and  $S$  is on, the energy is supplied to the load by  $L$ ,  $L_F$  and  $D_F$  respectively. Then, when  $S_F$  and  $S$  are both deactivated,  $L$  and  $D$  provide the energy directly to the load. The voltage relationships of DPP<sub>1</sub> and front-end converters are derived using a similar approach to that applied in the previous BCC analysis, and we have:

$$(1 - k_{KPP1})V_{DPP1} = (V_{fe} - V_{DPP1})k_{DPP1} \quad (5)$$

The relationship between  $V_{DPP1}$  and  $V_{fe}$  is given as:

$$k_{DPP1} = \frac{V_{DPP1}}{V_{fe}} \quad (6)$$

Thus, the voltage relationship between  $V_{fe}$  and  $V_{Bus}$  is expressed as:

$$k_{FE} = \frac{V_{fe}}{V_{Bus}} \quad (7)$$

### 3 TRANSFER FUNCTION MODEL OF MODULAR SP-DPPs

As the BCC and IBC circuits are both non-linear, only small AC signal transfer functions, linearised around the actual operating point, are derived.

### 3.1 Transfer function model for BCC

BCC<sub>1</sub> in Fig.1 is treated assuming that module PV<sub>1</sub> receives higher insolation, so S<sub>1</sub>-D<sub>2</sub> is active; other cases follow from symmetry. The analysis procedure is standard and uses a state-space variable vector  $x$  to describe the converter dynamics in on and off switching states; weighting the two obtained equations according to the duty ratio and summing them leads to an average equation of the BCC over one switching period. Then, transfer functions are derived by introducing a small ac perturbation to all relevant state variables in the averaged equation, followed by taking their Laplace transform. These transfer functions are expressed as the ratio between small changes in the PV voltages and in the duty ratio, known as  $\Delta v_{PV1}/\Delta k_{11}$ , or  $\Delta v_{PV2}/\Delta k_{11}$  are derived; detailed analysis is presented below.

For a BCC unit, the state vector  $x = [i_{L1} \ i_{L2} \ v_{PV1} \ v_{PV2} \ v_{CN}]^T$  represents the instantaneous currents and voltages of the BCC. The weighted average of the state-space equations for the on and off states of the converter yields a simplified dynamical equation averaged over one switching period,  $T_{sw}$ , expressed as:

$$\dot{x} = A_T x + B i_T + E_1 i_{PV1} + E_2 i_{PV2} \quad (8)$$

where,

$$A_T = \begin{bmatrix} 0 & 0 & \frac{1}{L_1} & 0 & -\frac{(1-k_{11})}{L_1} \\ 0 & 0 & 0 & -\frac{1}{L_2} & \frac{k_{11}}{L_2} \\ -\frac{1}{C_1} & 0 & 0 & 0 & 0 \\ 0 & \frac{1}{C_2} & 0 & 0 & 0 \\ \frac{(1-k_{11})}{C_n} & -\frac{k_{11}}{C_n} & 0 & 0 & 0 \end{bmatrix}, B = \begin{bmatrix} 0 \\ 0 \\ -1/C_1 \\ -1/C_2 \\ 0 \end{bmatrix},$$

$$E_1 = \begin{bmatrix} 0 \\ 0 \\ 1/C_1 \\ 0 \\ 0 \end{bmatrix} \text{ and } E_2 = \begin{bmatrix} 0 \\ 0 \\ 0 \\ 1/C_2 \\ 0 \end{bmatrix}$$

Vectors B, E<sub>1</sub> and E<sub>2</sub> are the state space input parameters of the BCC model, and  $i_{pv1}$ ,  $i_{pv2}$ ,  $i_T$  are respectively the currents flowing through each of the two chained PV modules, including their terminal current.  $K_{11}$  is the duty ratio of S<sub>1</sub>. Applying small ac perturbations in the steady-state dc variables, and omitting negligible products above first order, eq. (8) can be written as a small signal model given by:

$$\Delta x = A_T \Delta x + B \Delta i_T + E_1 \Delta i_{PV1} + E_2 \Delta i_{PV2} + H \Delta k_{11} \quad (9)$$

where,  $\Delta x = [\Delta i_{L1} \ \Delta i_{L2} \ \Delta v_{PV1} \ \Delta v_{PV2} \ \Delta v_{CN}]^T$ , and

$$H = \begin{bmatrix} \frac{V_{PV1} + V_{PV2}}{L_1} \\ \frac{V_{PV1} + V_{PV2}}{L_2} \\ 0 \\ 0 \\ \frac{I_{PV2} - I_{PV1}}{C_n} \end{bmatrix}$$

$\Delta i_{PV1}$  and  $\Delta i_{PV2}$  are the changes in currents of modules PV<sub>1</sub> and PV<sub>2</sub> respectively, at one operating point under a specified weather condition and can be given by:

$$\Delta i_{PV1} = -\frac{\Delta v_{PV1}}{R_{PV1}} \text{ and } \Delta i_{PV2} = -\frac{\Delta v_{PV2}}{R_{PV2}} \quad (10)$$

where,  $-1/R_{PV1}$  and  $-1/R_{PV2}$  are the gradients of the I-V characteristics of the PV panels at the operating point; thus, they vary with the MPP point. The overall simplified model can be obtained by substituting  $\Delta i_{PV1}$  and  $\Delta i_{PV2}$  in eq. (9) by eq. (10):

$$\Delta x = A_T \Delta x + B \Delta i_T + H \Delta k_{11} \quad (11)$$

$$A_T = \begin{bmatrix} 0 & 0 & \frac{1}{L_1} & 0 & -\frac{(1-k_{11})}{L_1} \\ 0 & 0 & 0 & -\frac{1}{L_2} & \frac{k_{11}}{L_2} \\ -\frac{1}{C_1} & 0 & -\frac{1}{R_{PV1}C_1} & 0 & 0 \\ 0 & \frac{1}{C_2} & 0 & -\frac{1}{R_{PV2}C_2} & 0 \\ \frac{(1-k_{11})}{C_n} & -\frac{k_{11}}{C_n} & 0 & 0 & 0 \end{bmatrix} \text{ and}$$

$$H = \begin{bmatrix} \frac{V_{PV1} + V_{PV2}}{L_1} \\ \frac{V_{PV1} + V_{PV2}}{L_2} \\ 0 \\ 0 \\ \frac{V_{PV2}}{R_{PV2}C_n} - \frac{V_{PV1}}{R_{PV1}C_n} \end{bmatrix}$$

The variation in voltage across PV<sub>1</sub> is then expressible as:

$$\Delta v_{PV1} = [0 \ 0 \ 1 \ 0 \ 0] \Delta x = Z_1 \Delta x \quad (12)$$

Similarly,  $\Delta v_{PV2} = [0 \ 0 \ 0 \ 1 \ 0] \Delta x = Z_2 \Delta x$ . The BCC's passive elements are selected such that  $L_1=L_2$  and  $C_1=C_2$ . The function of the terminal DPP<sub>1</sub> converter is to deliver the total extracted power to the bus side. Therefore, the DPP<sub>1</sub>'s power rating would be proportional to the difference in voltage between the bus and BCC<sub>1</sub> unit. In this case, outer DPP converters do not need to handle the total power generated PV modules; thus, they have slower dynamics than that of the inner BCCs. Generally, more power handling implies slower dynamics on the system.

This indicates that the terminal current ripple,  $\Delta i_T$ , which is controlled by the BCC, can be approximated to be almost zero, whereas the terminal voltage remains constant, i.e.  $V_{T1} = V_{PV1} + V_{PV2}$ . Hence,  $B \Delta i_T$  in eq. (11) is eliminated. The control-to-input voltage transfer function (i.e.  $\Delta v_{PV1}$  and  $\Delta k_{11}$ ) is given by:

$$G_1(s) = \frac{\Delta v_{PV1}}{\Delta k_{11}} = Z_1 (sI - A_{sm}^*) H$$

$$= -\frac{b_3 s^3 + b_2 s^2 + b_1 s + b_0}{a_5 s^5 + a_4 s^4 + a_3 s^3 + a_2 s^2 + a_1 s + a_0} V_{T1} \quad (13)$$

Where, coefficients of both numerator and denominator are all listed in appendix. In the above derivation, it is assumed that  $L=L_1=L_2$ ,  $C=C_1=C_2$ . The second transfer function between PV<sub>2</sub> voltage ( $\Delta v_{PV2}$ ) and  $\Delta k_{11}$ , i.e.  $G_2(s) = \frac{\Delta v_{PV2}}{\Delta k_{11}}$ , is similar to eq. (13) having the same denominator, but the coefficients of the numerator part are different and also given in appendix, expressed as:

$$G_2(s) = \frac{\Omega_3 s^3 + \Omega_2 s^2 + \Omega_1 s + \Omega_0}{a_5 s^5 + a_4 s^4 + a_3 s^3 + a_2 s^2 + a_1 s + a_0} V_{T1} \quad (14)$$

The denominator in both equations (13) and (14) respectively implies that all poles are located on the left-hand side of the s-plane; thus, both transfer functions  $G_1(s)$  and  $G_2(s)$  are stable 5<sup>th</sup> order systems. Most crucially, the former might have right-hand plane zeros exhibiting non-minimum phase features. This can be caused as either  $b_1$  or  $b_2$  may become negative when  $\frac{(1-K_{11})}{R_{PV1}} > \frac{K_{11}}{R_{PV2}}$  in the two derived transfer functions. Therefore,  $C_n$  and  $L$  components should be carefully selected to ensure that  $b_1$  and  $b_2$  are always  $> 0$  under all possible weather conditions of  $k_{11}$ ,  $R_{PV1}$  and  $R_{PV2}$ .

### 3.2 Transfer function model for IBC

Similarly to the BCC case, the generalised transfer function model  $G_3(s)$  of the IBC is derived here by combining two small-signal models; where one is between the input voltage  $\Delta v_{T1}$  and the middle across  $C_{TF}$  (i.e.  $\Delta v_{fe}$ ), and the other is the relationship between  $\Delta v_{fe}$  and duty ratio  $\Delta k_{DPP1}$  as seen in Fig. 2, given as:

$$= -\frac{2V_{Bus}C_{TF}L_F s^2 + I_{T1}(C_{TF}L_F(1-K_{FE})^2 - L_F(K_{FE})^2)s + V_{Bus}}{\alpha_2 s^4 + \alpha_1 s^2 + 1}$$

where, the denominator coefficients are expressed as:

$$\alpha_1 = 2C_{TF}L_F + C_F(L_F(1-K_{FE})^2 + L_F(K_{FE})^2),$$

$$\alpha_2 = C_{TF}C_F L_F^2$$

The above analysis assumes that  $L=L_F$  and  $C_0=C_{T1}=C_F$ . The negative sign in the transfer function  $G_3(s)$  indicates that the terminal BCC voltage  $V_{T1}$  is varying inversely with the DPP1 duty ratio  $K_{DPP1}$ . The IBC transfer function depends on the values of the circuit elements, most importantly on the circuit operating points, i.e.  $V_{T1}$  and  $K_{FE}$ .

## 4 DESIGN CONSIDERATIONS OF SP-DPPS CONVERTERS

Design of the BCC involves the selection of proper values for the inductor  $L$  (i.e.  $L_1=L_2=L$ ) and capacitors  $C$  and  $C_n$ , where ( $C_1=C_2=C$ ). Also, passive components belonging to IBC, including  $L_F$ ,  $C_F$  and  $C_{TF}$  need to be appropriately selected. The selection criteria are:

- To minimise voltage and current ripples at their steady states.
- to achieve good (and stable) transient responses.

### 4.1 Selecting C and $C_F$

For the first requirement to be satisfied, ripples magnitudes of both output voltage and inductor current are evaluated.

The output voltage ripple of the BCC is expressed as:

$$\Delta v_o = \frac{\Delta q_0}{C_2} = \frac{\Delta i_{L2}}{8C_2 F_s} \quad (15)$$

where,  $\Delta q_0$  is the surplus charge accumulated in capacitor  $C_2$  during the charging state. The output inductor current ripple during the switching off period is expressed as:

$$\Delta i_{L2} = \frac{(1-K_{11})V_o}{L_2 F_s} \quad (16)$$

Substituting  $\Delta i_{L2}$  in (15) by (16) yields:

$$\Delta v_o = \frac{(1-K_{11})}{8C_2 L_2 F_s^2} V_o = \frac{\pi^2(1-K_{11})}{2} \left(\frac{F_c}{F_s}\right)^2 V_o \quad (17)$$

where, the cut-off frequency for the low pass filter L<sub>2</sub>-C<sub>2</sub> is:

$$F_c = \frac{1}{2\pi\sqrt{L_2 C_2}} \quad (18)$$

The output voltage ripple  $\Delta v_o$  can be reduced by choosing low-pass filter parameters such that  $F_s \gg F_c$ .

$L_2$  and  $C_2$  dictate appropriate  $F_c$ ; hence these components values may be pre-determined based on the compromise between the ripple requirements and physical converter size. Likewise, the value of  $C_F$  for IBC is calculated as follows:

$$C_F = \frac{(1-K_F) V_o}{8L_F F_s^2 \Delta V_o} \quad (19)$$

However, values of  $L$  and  $C_n$  for BCC, including those of  $C_{TF}$  and  $L_F$  for IBC must be designed carefully for satisfying the desired performance of the transient response.

### 4.2 Selecting L, $C_n$ , $C_{TF}$ and $L_F$

The aim here is to achieve a good transient performance with minimal oscillations, overshoot and settling time. As seen in both equations (13) and (14), the SP-DPPs system may present non-minimum phase characteristics depending on  $L$ ,  $C_n$ ,  $L_F$ ,  $C_{TF}$  in addition to the duty cycle used.

The result is that a sudden increase in either  $K_{11}$  or  $K_{DPP1}$  may not lead to an immediate rise in their associated  $i_{L1}$  and  $i_{LF}$ , respectively. Instead, reducing the switch-off period causes a reduction in the energy transferred to  $C_n$  and  $C_{TF}$ , and hence the output. Therefore, the terminal array current, and the individual PV voltages for the system shown, initially dip down before they increase and stabilise at higher steady-state values. Such non-minimum phase behaviour may lead to instability in the model-based controller. The unstable zero may also reduce the damping of the SP-DPPs circuit. The optimal solution can be achieved by predicting the output array current, including PV voltage responses for different  $L$ ,  $C_n$ ,  $L_F$  and  $C_{TF}$ ; and selecting the parameters for minimum variance between the current response and its desired value. For preventing the transient performance from being affected by the non-minimum phase feature, a weighted cost function is introduced as:

$$E = \sum_{i=1}^{i=j} (V_{PVm}^* - wV_{PVm}[nT_n])^2 \quad (20)$$

where,  $V_{PVm}$  is the ideal voltage for the individual PV modules (i.e.  $m=1$  to 4),  $V_{PVm}[nT_n]$  is the n-th sample of the voltage response due to the variation of the duty ratio, and  $j$  is the total number of samples selected. Thus, weighting factor  $w$  values are carefully chosen so that the variance caused by non-minimum phase feature is much less than that due to the PV voltage transient response. This is only valid when  $V_{PVm}[nT_n] < V_{PVm}(0)$ , including other cases when  $V_{PVm}[nT_n] > V_{PVm}(0)$ ,  $w$  is always equal to 1. Then, determination of the Error  $E$  can be carried out for a range of  $L$ ,  $C_n$ ,  $L_F$  and  $C_{TF}$  combinations while using the same pair of  $C$  and  $C_F$  values calculated in the previous

sub-section. The optimal  $L$ ,  $C_n$ ,  $L_F$  and  $C_{TF}$  should be the case which gives the minimum  $E$  value.

## 5 SIMULATION RESULTS AND DISCUSSIONS

The 187.47 W modular SP-DPPs converters system with the specifications shown in Table 1, has been designed based on the above proposed procedure. Subsequently,  $C$  and  $C_F$  are set to 20.0  $\mu\text{F}$  and 10.0  $\mu\text{F}$  respectively for  $K_{FE} = 0.29$ ,  $K_{DPP1} = K_{DPP2} = 0.21$  and  $K_{I1} = 0.5$ . For optimisation of  $L$ ,  $C_n$ ,  $L_F$  and  $C_{TF}$  values, a set of cost function values is evaluated for which  $w = 0.685$  for  $V_{PVm}[nT_n] < V_{PVm}(0)$  and  $w = 1$  otherwise. For the sum of squared errors in eq. (20) for all valid element values;  $C_{TF}$ ,  $C_n$  ranging from 5.0 to 40.0  $\mu\text{F}$  while  $L$ ,  $L_F$  both from 4.0 to 10.0 mH.

### 5.1 Design verifications

To validate the proposed design, five sets of parameters notated as  $A_1$  to  $A_5$  was simulated via **MATLAB-SIMULINK**. For each case, terminal array current response of the SP-DPPs system due to the same pattern of duty ratio change (i.e. from  $K_{I1} = 0.475$  to  $K_{I1} = 0.5$ ) are shown in Fig. 3. Their performance factors are listed in Table 2 for comparison.

**Table I:** Design specifications for SP-DPPs array system

Parameters	Symbols	Values
Bus voltage	$V_{Bus}$	35 V
Front-End voltage	$V_{fe}$	10 V
DPP voltage	$V_{DPP}$	2 – 4 V
PV open-circuit voltage	$V_{OC}$	20 V
PV short-circuit current	$I_{SC}$	3.3 A
Switching frequency	$F_S$	20 KHz
Maximum output voltage ripple	$\Delta V_o$	2%
Maximum output current ripple	$\Delta i_o$	2%

For **case A1**,  $L = 4.0$  mH,  $L_F = 4.0$  mH,  $C_n = 6.0$   $\mu\text{F}$  and  $C_{TF} = 8.0$   $\mu\text{F}$ . Although, the array current transient response presents high overshoot of 5.7 percent due to the non-minimum phase effect, it takes relatively short time of approximately 2.4 ms to settle into its steady state. On the other hand, the magnitude ripple of steady state is much larger than the desired 2%.

In comparison, **case A2** shows slightly smaller overshoot of 3.8% while the percentage of steady-state ripple is below the 2% limit. However, its step response is oscillatory and take 15 ms to settle down. Also, the  $E$  value is the highest among all cases.

**Case A3** is less oscillatory compared to the previous two cases which is desirable. However, the transient response is still subjected to low levels of oscillations and takes long time to settle down. **Case A4** has better response compared to the previous cases apart from its initial spikes. However, it takes more time than that of case  $A_1$  to settle down. **Case A5** presents the lowest  $E$  value with almost negligible overshoot, its transient time response is about 2.1 ms, including the steady-state ripple of within 2%. Therefore, this has the best transient performance.

### 5.2 Application to the MPP tracking of 2x2 PV array

The SP-DPPs converters scheme shown in Fig. 1 above has been used for the Maximum Power Point (MPP) tracking for a 2x2 PV array system, and to validate the proposed design method.

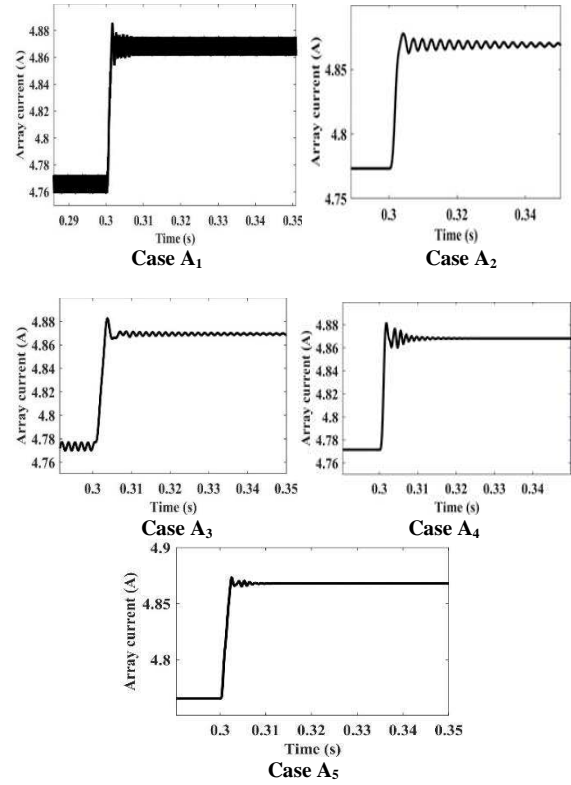


**Fig. 3:** Transient responses due to step change in duty ratio

- (a) **Case A1** –  $L = 4$  mH,  $L_F = 4$  mH,  $C_n = 6$   $\mu\text{F}$  &  $C_{TF} = 8$   $\mu\text{F}$
- (b) **Case A2** –  $L = 8$  mH,  $L_F = 8$  mH,  $C_n = 6$   $\mu\text{F}$  &  $C_{TF} = 8$   $\mu\text{F}$
- (c) **Case A3** –  $L = 8$  mH,  $L_F = 8$  mH,  $C_n = 8$   $\mu\text{F}$  &  $C_{TF} = 15$   $\mu\text{F}$
- (d) **Case A4** –  $L = 4$  mH,  $L_F = 4$  mH,  $C_n = 8$   $\mu\text{F}$  &  $C_{TF} = 15$   $\mu\text{F}$
- (e) **Case A5** –  $L = 8$  mH,  $L_F = 8$  mH,  $C_n = 10$   $\mu\text{F}$  &  $C_{TF} = 35$   $\mu\text{F}$

**Table II:** Transient and steady-state performance for SP-DPPs circuit system

Points	Ripple $\Delta i_o$ %	Overshoot %	Settling time ms	$E$ $10^5 \text{ V}^2$
A1	20	5.7	2.4	1.3210
A2	0.45	3.8	15	1.3260
A3	0.45	4.3	11	1.3197
A4	0.39	4.4	6	1.3191
A5	<b>0.19</b>	<b>0.09</b>	<b>2.1</b>	<b>1.3158</b>

The MPP tracking can be achieved by adjusting the duty ratios of both BCCs and IBC converters. Thus, this can be done using Perturb and Observe (P&O) algorithm, which is simple to implement, though it may lead to unnecessary voltage oscillations [6]. Therefore, the above converters should be stable and fast, which is desirable enough to reduce such effect. Note, the sampling time used for P&O method is  $1 \times 10^{-5}$  s for inner BCCs and 0.01 s for outer DPPs.

The designed circuit components in the previous section has been also applied for MPPT of SP-DPPs system. Hence, the simulated array current and the individual PV voltage responses for different levels of sunlight intensity are all shown in Figs. 4 and 5 respectively. As shown in Fig. 4, after 0.2 s, modules  $PV_2$ ,  $PV_3$  and  $PV_4$  each experiences a drop in solar irradiation value at 0.2 s, 0.3 s and 0.4 s respectively, while  $PV_1$  is at the standard conditions. For the voltage responses, before  $t = 0.2$  s, the solar intensity on both  $PV_1$  and  $PV_3$  is at 1000  $\text{W}/\text{m}^2$  while that on  $PV_2$  and  $PV_4$  is at 800  $\text{W}/\text{m}^2$ . Hence,

their measured voltages are initially at about 16.88 V for PV<sub>1</sub> and PV<sub>3</sub>, and 16.33 V for PV<sub>2</sub> and PV<sub>4</sub> respectively.

As seen from the voltage waveforms in Fig. 5(a), the corresponding transient responses using the best set of components in case A<sub>5</sub>, present a negligibly small overshoot whereas the steady-state ripple magnitudes are well below 2%.

Therefore, the system subsequently undergoes 3 duty ratio adjustments between  $t = 0.2$  and  $t = 0.4$  second. Throughout this period, the duty cycles of BCCs and IBCs reduces steadily and are determined by the inner and outer P&O control algorithms. When  $t = 0.4$  s, the alteration of duty cycles stops since the four PV voltages settle down to their new MPP values.

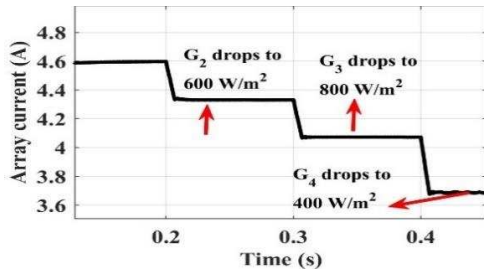


Fig. 4: Terminal array current response due to MPP tracking

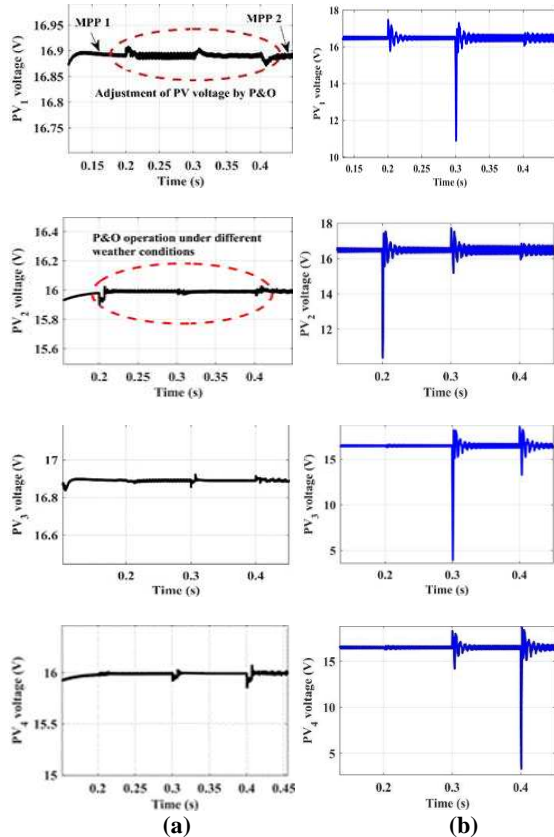


Fig. 5: Voltage Responses of PV modules due to MPP tracking: (a) PV voltages generated using set of components in A<sub>5</sub>; (b) PV voltages generated using set of components in A<sub>2</sub>

It can also be revealed that for every change of any of the PV voltages, the transient states last about 10 ms; hence, voltage spikes are not significant. On the other

hand, the corresponding voltage ripples remain to be low.

On the other hand, Fig. 5(b) presents the four PV voltage responses using set of components considered in case A<sub>2</sub>. For MPPT operation, all voltage responses have shown significant undershoots provided that they are oscillatory and their magnitude ripples above the required 2 percent.

When MPP is in action, case A<sub>5</sub> gives minimal voltage fluctuations while A<sub>2</sub> results in higher ones which are undesirable. Therefore, the obtained results using A<sub>5</sub> have shown that the optimised design scheme fully satisfies the performance requirements for the Series-Parallel PV array system.

## 6 CONCLUSIONS

A design approach has been proposed for series-parallel connected PV arrays in which maximum power point tracking is realized using differential power processing to reduce losses. The scheme uses bidirectional Cuk converters and inverted buck converters for setting optimum PV module currents and voltages respectively. Transfer functions of the converters were derived in frequency domain using linearization and state space time averaging of the system equations. These were used to develop design criteria for fast settling and freedom from oscillations and limiting the undershoot which arises from a non-minimum phase response.

A representative design was found with excellent transient responses and settling time around 10ms. This clearly makes MPPT by a simple-perturb-and-observe scheme feasible, even when substantial numbers of converters and modules need simultaneous tracking. Correct operation of such a scheme was verified by a full non-linear simulation of a complete system. On the other hand, when this converter has been designed with the scheme proposed in this paper, other more complex MPPT schemes using feedback controller, such as those employing model-based technique can be avoided.

## 7 REFERENCES

- [1] Olalla, C.; Maksimovic, D.; Deline, C.; Martinez-Salamero, L. Impact of Distributed Power Electronics on the Lifetime and Reliability of PV Systems. *Prog. Photovolt. Res. Appl.* 2017, 25, 821–835.
- [2] H. Lee and K. A. Kim, "Design Considerations for Parallel Differential Power Processing Converters in a Photovoltaic-Powered Wearable Application," *Energies*, vol. 11, pp. 1-17, 2018.
- [3] F. S. Bagci, Y. Liu, and K. A. Kim, "Low-Power Photovoltaic Energy Harvesting with Parallel Differential Power Processing Using a SEPIC," in 2019 IEEE Applied Power Electronics Conference and Exposition (APEC), 2019, pp. 2008-2014.
- [4] H. Zhou, J. Zhao, and Y. Han, "PV Balancers: Concept, Architectures, and Realization," *IEEE Transactions on Power Electronics*, vol. 30, pp. 3479-3487, 2015.
- [5] Etarhouni, M, Chong, B and Zhang, L (Accepted: 2020) Series-Parallel Differential Power Processing Scheme for Maximised Power Extraction from Mismatched Photovoltaic Panels. In: *IET Proceedings of the 10th International Conference on Power Electronics, Machines and Drives (PEMD 2020)*. (In Press).

[6] B. V. P. Chong and L. Zhang, "Controller design for integrated PV-converter modules under partial shading conditions," *Solar Energy*, vol. 92, pp. 123-138, 2013.

[7] Niazi, K.A.K.; Yang, Y.; Nasir, M.; Sera, D. Evaluation of Interconnection Configuration Schemes for PV Modules with Switched-Inductor Converters under Partial Shading Conditions. *Energies* 2019, 12, 2802.

## 8 APPENDICES

The coefficients of numerator and denominator parts of equations (13) and (14) respectively are expressed as:

$$\begin{aligned} b_3 &= CC_nL, b_2 = \frac{C_nL}{R_{PV2}} + CL(1 - K_{11}) \left( \frac{(1-K_{11})}{R_{PV1}} - \frac{K_{11}}{R_{PV2}} \right), \\ b_1 &= C_n + CK_{11} + \frac{L(1-K_{11})}{R_{PV2}} \left( \frac{(1-K_{11})}{R_{PV1}} - \frac{K_{11}}{R_{PV2}} \right), \\ b_0 &= \frac{(1-K_{11})^2}{R_{PV1}} + \frac{K_{11}^2}{R_{PV2}} \end{aligned} \quad (A1)$$

$$\begin{aligned} a_5 &= (CL)^2C_n, a_4 = CC_nL^2 \left( \frac{1}{R_{PV1}} + \frac{1}{R_{PV2}} \right), \\ a_3 &= C_nL \left( 2C + \frac{L}{R_{PV1}R_{PV2}} \right) + C^2L(K_{11}^2 + (1 - K_{11})^2), \\ a_2 &= L \left( C_n + CK_{11}^2 + C(1 - K_{11})^2 \left( \frac{1}{R_{PV1}} + \frac{1}{R_{PV2}} \right) \right), \\ a_1 &= C_n + (K_{11}^2 + (1 - K_{11})^2) \left( C + \frac{L}{R_{PV1}R_{PV2}} \right) \text{ and} \\ a_0 &= \frac{(1-K_{11})^2}{R_{PV1}} + \frac{K_{11}^2}{R_{PV2}} \end{aligned} \quad (A2)$$

$$\begin{aligned} \Omega_3 &= CC_nL, \Omega_2 = \frac{C_nL}{R_{PV1}} + CLK_{11} \left( \frac{K_{11}}{R_{PV2}} - \frac{(1-K_{11})}{R_{PV1}} \right), \\ \Omega_1 &= C_n + C(1 - K_{11}) + \frac{LK_{11}}{R_{PV1}} \left( \frac{K_{11}}{R_{PV2}} - \frac{(1-K_{11})}{R_{PV1}} \right) \text{ and} \\ \Omega_0 &= \frac{(1-K_{11})^2}{R_{PV1}} + \frac{K_{11}^2}{R_{PV2}} \end{aligned} \quad (A3)$$